Chemical Science

ROYAL SOCIETY OF CHEMISTRY

EDGE ARTICLE

View Article Online
View Journal | View Issue

Cite this: *Chem. Sci.*, 2024, **15**, 6160

All publication charges for this article have been paid for by the Royal Society of Chemistry

Vibrational spectroscopy and dissociation dynamics of cyclohexyl hydroperoxide†

Tarun Kumar Roy, [a] Yujie Qian, [a] Elizabeth Karlsson, [a] Rawan Rabayah, [a] Christopher A. Sojdak, [a] Marisa C. Kozlowski, [a] Tolga N. V. Karsili [b] and Marsha I. Lester *[a]

Received 8th January 2024
Accepted 19th March 2024

DOI: 10.1039/d4sc00151f

rsc.li/chemical-science

Organic hydroperoxides (ROOH) are ubiquitous in the atmospheric oxidation of volatile organic compounds (VOCs) as well as in low-temperature oxidation of hydrocarbon fuels. The present work focuses on a prototypical cyclic hydroperoxide, cyclohexyl hydroperoxide (CHHP). The overtone OH stretch ($2\nu_{OH}$) spectrum of jet-cooled CHHP is recorded by IR multiphoton excitation with UV laser-induced fluorescence detection of the resulting OH products. A distinctive IR feature is observed at 7012.5 cm^{-1}. Two conformers of CHHP are predicted to have similar stabilities (within 0.2 kcal mol^{-1}) and overtone OH stretch transitions ($2\nu_{OH}$), yet are separated by a significant interconversion barrier. The IR power dependence indicates that absorption of three or more IR photons is required for dissociation of CHHP to cyclohexoxy (RO) and OH radical products. Accompanying high-level single- and multi-reference electronic structure calculations quantitatively support the experimental results. Calculations are extended to a range of organic hydroperoxides to examine trends in bond dissociation energies associated with RO + OH formation and compared with prior theoretical results.

1 Introduction

Organic hydroperoxides (ROOH) are formed in the oxidation of volatile organic compounds (VOCs) in the atmosphere or during combustion.[1,2] The primary VOC generally reacts with hydroxyl (OH) radicals to form an alkyl radical that promptly reacts with O_2 to generate an alkylperoxy (RO_2) radical.[3,4] The fate of the nascent RO_2 is heavily dependent on its molecular structure as well as the temperature and pressure of the surroundings.[5,6]

In the atmosphere, the dominant removal of nascent RO_2 radicals in pristine environments is by reaction with HO_2, which forms lower volatility ROOH compounds.[7–10] Alternatively, the RO_2 radical may undergo hydrogen atom transfer (HAT) to form a carbon-centered hydroperoxyalkyl radical (˙QOOH),[5,6,11–13] which generally undergoes unimolecular decay or reacts with O_2 to form ˙OOQOOH. Sequential repetition of HAT and O_2 addition, termed autoxidation, may eventually form a highly oxidized ROOH compound, which has lower volatility than the precursor VOC.[14–19] Such compounds are implicated in the formation of secondary organic aerosols, which affect radiative forcing in the atmosphere and impact public health.[20–22] In contrast, reaction with HO_2 represents a minor sink for RO_2 radicals formed during low temperature combustion (such as in modern-day vehicle engines).[23–26] Under these conditions, the higher temperatures and pressures usually promote intramolecular HAT to form ˙QOOH radicals which play a vital role in fuel autoignition.[14,23–36]

Given their significance in atmospheric and combustion chemistry, a thorough understanding of spectroscopy and dissociation dynamics of ROOH compounds is needed. Prior studies have focused on the vibrationally mediated photodissociation dynamics of hydrogen peroxide and simple organic peroxides.[37–41] The fundamental OH stretch and various overtone OH stretch transitions of H_2O_2 and its partially deuterated analogue HOOD have been characterized with a variety of techniques.[42] Excitation at $6\nu_{OH}$ provides sufficient energy to promote O–O bond dissociation to form OH $X^2\Pi$ fragments. These studies reveal that *ca.* 11% of the resulting OH fragments formed are vibrationally excited. This is in stark contrast to near UV photodissociation studies of H_2O_2 and organic hydroperoxides, which predominantly yield rovibrationally cold OH products.[43–48]

Studies have been extended to *tert*-butyl hydroperoxide (TBHP), where a sequence of OH-stretch transitions from the fundamental through the fifth overtone has been characterized.[40,41] Recent work revealed a strong feature at ~7017 cm^{-1} arising from the first overtone OH stretch ($2\nu_{OH}$), which is heavily coupled to COOH torsion.[49,50] The $\nu_{OH} = 0$ and $\nu_{OH} = 2$ levels undergo tunneling splitting due to a double-minimum potential energy well along the COOH torsional coordinate.

[a]*Department of Chemistry, University of Pennsylvania, Philadelphia, PA 19104-6323, USA. E-mail: milester@sas.upenn.edu*

[b]*Department of Chemistry, University of Louisiana, Lafayette, LA, USA*

† Electronic supplementary information (ESI) available. See DOI: https://doi.org/10.1039/d4sc00151f

OH radical products are detected following $\nu_{OH} = 2$ excitation of TBHP, arising from the absorption of three or more photons of the same wavelength to promote dissociation, while $\nu_{OH} = 6$ excitation results in single photon dissociation. The prevailing mechanism for dissociation involves rapid intramolecular vibrational energy redistribution (IVR) followed by O–O bond fission to form OH + RO radical products. The timescale for dissociation is controlled by unimolecular decay along a barrierless potential. Analogous vibrationally activated dissociation is expected for other ROOH compounds with greater molecular complexity. Bach and Schlegel undertook a systematic computational study of various organic hydroperoxides, revealing bond dissociation energies on the order of 45 kcal mol^{-1}, which are consistent with experimental values for a range of hydroperoxides.[51,52]

This study characterizes the first overtone OH stretch ($2\nu_{OH}$) of cyclohexyl hydroperoxide (cyc–C_6H_{11}O–OH, CHHP) and its multiphoton dissociation dynamics with OH products. A new synthetic approach is introduced to safely generate CHHP from cyclohexene. The present work builds on a recently reported high-resolution rotational spectroscopy study of the equatorial and axial conformers of CHHP in a Ne expansion (CHHP 1 and 2, respectively), which determined their structures and mapped out the conformational landscape involving torsional motions of the –OOH group.[53] Another recent study focused on the synthesis of a wide range of organic hydroperoxides, including CHHP, and determined their absolute photoionization cross sections and resultant fragmentation (–OOH loss) channels.[54] The present experimental study is complemented by high-level single- and multi-reference electronic structure calculations for CHHP and a range of other hydroperoxides.

2 Methods

2.1 Synthesis

A new synthetic approach was chosen for preparing cyclohexyl hydroperoxide (CHHP) to avoid the storage of large quantities of CHHP due to the explosive nature of organic hydroperoxides. It was hypothesized that protecting the peroxide with an appropriate silane group would increase the molecular mass and greatly decrease the risk of unexpected detonation of the material.[55] Specifically, as shown in Scheme 1, cobalt-catalyzed silylperoxidation of cyclohexene directly yielded the triethylsilyl protected peroxide, (cyclohexylperoxy) triethylsilane, in excellent yields on a multigram scale.[56] From (cyclohexylperoxy) triethylsilane, conventional deprotection with pyridine·HF yielded very pure cyclohexyl hydroperoxide in poor yields. However, the poor yields of this transformation were vastly offset by rapid reaction times and more importantly the avoidance of storing bulk quantities of organic hydroperoxide, thus improving the safety of this approach. Extensive details on the synthetic preparation and analytical characterization of CHHP are presented in the ESI (ESI, see Section S1 and Fig. S1–S4†).

2.2 Spectroscopic methods

The experimental method is similar to that used in a recent IR spectroscopic study of TBHP.[49] Freshly synthesized CHHP is seeded in Ar carrier gas at a pressure of 25 psig. The gas mixture is pulsed through a solenoid valve and an affixed quartz capillary tube (~25 mm length and 1 mm ID) into a vacuum chamber. The resultant supersonic expansion cools CHHP to a rotational temperature of *ca.* 10 K. Counter propagating IR and UV beams are spatially overlapped and intersect the gas mixture in the collision-free region *ca.* 1 cm downstream from the exit of the capillary. Multiphoton IR excitation of jet-cooled CHHP in the overtone OH stretch region ($2\nu_{OH}$) results in dissociation to OH $X^2\Pi_{3/2}$ ($v = 0$) radical products that are detected. The tunable IR beam (with powers up to *ca.* 28 mJ per pulse) is the signal output of an optical parametric oscillator/amplifier (OPO/OPA, LaserVision; 0.9 cm^{-1} bandwidth) pumped using an unseeded Nd:YAG laser (1064 nm, Continuum Surelite EX, 5 Hz). The OH radical products are probed *via* laser-induced fluorescence (LIF) on the $A^2\Sigma^+$–$X^2\Pi_{3/2}$ (1,0) $Q_1(3.5)$ transition at 282 nm utilizing UV radiation (*ca.* 1 mJ per pulse) generated with the frequency-doubled output of a Nd:YAG (EKSPLA NL300; 532 nm, 10 Hz) pumped dye laser (Continuum ND6000, Rhodamine 590 dye).

The fluorescence emitted on the OH $A^2\Sigma^+$–$X^2\Pi_{3/2}$ (1,1) transition is detected using a gated photomultiplier tube (Electron Tubes 9813QB) and preamplified. Data acquisition involves an active background subtraction scheme (IR on – IR off) to remove a weak OH LIF background signal that arises from UV photodissociation of CHHP at 282 nm.

2.3 Computational methods

The ground state minimum energy geometry for a range of ROOH compounds and their associated anharmonic normal mode wavenumbers were computed at the B2PLYP-D3/cc-pVTZ level of theory. Equivalent calculations were carried out for the OH and RO radicals formed upon O–O bond fission. Single point energies for the resultant optimized geometries were calculated at the CCSD(T)-F12/cc-pVTZ-F12 level of theory. Bond dissociation energies associated with RO + OH formation (D_0[RO–OH]) as well as the energy profile along the equatorial to

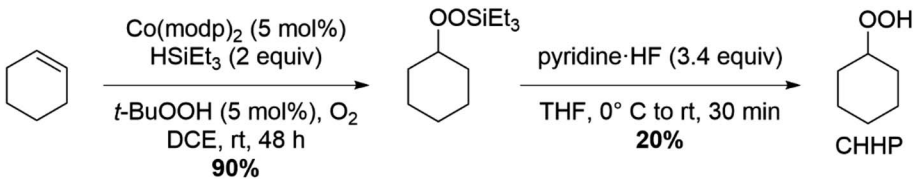

Scheme 1 Synthetic route to generate cyclohexyl hydroperoxide (CHHP).

axial isomerization pathway were calculated using the CCSD(T)-F12 energies and harmonic zero-point energies (ZPEs) from the B2PLYP-D3/cc-pVTZ calculations described above. Additional bond dissociation energies for CHHP and other organic hydroperoxides were computed using the W1BD composite method,[57] which is known to provide highly accurate thermochemical data within chemical accuracy (*ca.* 1 kcal mol^{-1}).

The ground state relaxed potential energy (PE) profile of CHHP along the O–O stretch coordinate (R_{O-O}) was calculated with single-state complete active space second-order perturbation theory (CASPT2) coupled to Dunning's aug-cc-pVTZ basis set (henceforth CASPT2/AVTZ). This was achieved by fixing R_{O-O} at various values across the range 1.0–5.6 Å and allowing the remainder of the nuclear frameworks to relax to their respective minimum energy configurations. These were based on a 4-state averaged complete active space self-consistent field (SA4-CASSCF) wavefunction employing the same basis set. An active space of 6 electrons in 4 orbitals was utilized to describe all significance short- and long-range interactions of the system while maintaining an appropriate computational expense. The active orbitals are displayed in Fig. S5,† while the orbital occupancies of the ground and excited electronic states of CHHP are shown in Fig. S6 of the ESI.† An imaginary level shift of 0.4 E_H was used to aid convergence and to mitigate the involvement of intruder states.

The B2PLYP-D3 and W1BD calculations were performed using Gaussian 16 software suite[58] while the CCSD(T)-F12 and CASPT2 calculations were performed using the Molpro computation package.[59–61]

3 Results and discussion

Cyclohexyl hydroperoxide (CHHP) is predicted to have two stable chair conformations with the –OOH group in an equatorial or axial position of the ring. The present calculations indicate that the equatorial conformer is more stable by 0.2 kcal mol^{-1}. A prior investigation of the conformational landscape of CHHP (B3LYP-D3(BJ)/def2-TZVP) also found the equatorial conformer to be lower in energy, although by *ca.* 1 kcal mol^{-1}.[53] As illustrated in Fig. 1, the interconversion between equatorial and axial configurations involves a sequence of geometry changes. The equatorial conformer initially transforms into a twist-boat configuration through a half-chair transition state (TS) barrier of 11.5 kcal mol^{-1} (Table S1†). Subsequently, interconversion between the two twist-boat configurations occurs *via* a TS (*ca.* 1.5 kcal mol^{-1}) with a boat geometry. The second twist-boat configuration converts into the axial conformer through another half-chair TS.

The relative stability of the equatorial and axial conformers suggests that both conformers will be populated with an estimated 60 : 40 ratio in favor of the equatorial conformer based on a room temperature Boltzmann population distribution. The significant TS barriers separating the equatorial and axial conformations indicate that both conformers will be populated under jet-cooled conditions, as found in a recent rotational spectroscopy study.[53] In addition, the earlier study anticipated a second equatorial conformer (0.67 kcal mol^{-1} higher in energy) associated with internal rotation about the C–O bond (not shown in Fig. 1) that was not observed, presumably due to relaxation *via* a low torsional barrier of only 4 kcal mol^{-1}.[53]

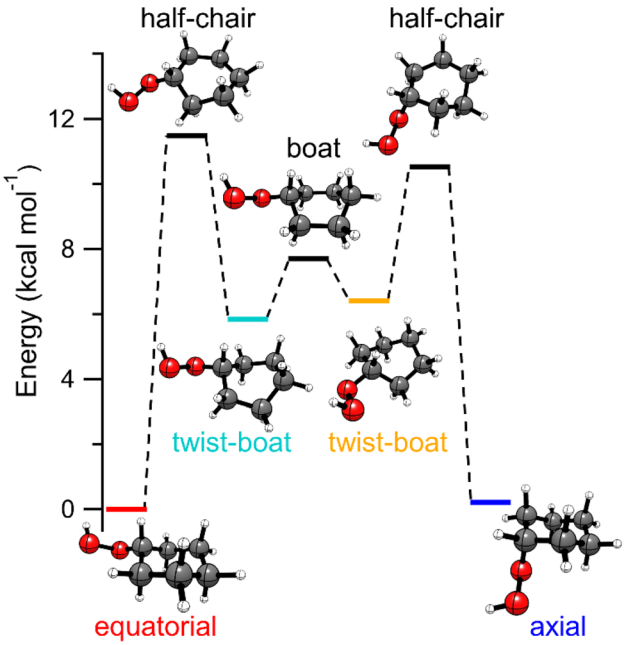

Fig. 1 Energy profile connecting the equatorial and axial conformers of CHHP calculated at the CCSD(T)-F12/cc-pVTZ-F12//B2PLYP-D3/cc-pVTZ level of theory.

In this study, we examine the IR spectrum of CHHP in the first overtone OH stretch region ($2\nu_{OH}$), guided by electronic structure calculations performed at the B2PLYP-D3/cc-pVTZ level of theory/basis. The equatorial and axial structures of CHHP are optimized, and the anharmonic vibrational frequencies and IR absorption intensities (Table S2†) are calculated at these geometries using second-order vibrational perturbation theory (VPT2). The first overtone OH stretch for the equatorial and axial conformers of CHHP is predicted at 7006 and 6999 cm^{-1}, respectively, as shown in Fig. 2. IR transitions associated with both equatorial and axial conformers of CHHP are anticipated based on the significant TS barrier separating the two conformers (Fig. 1) and the observation of both conformers in the recent rotational spectroscopy study.[53]

The IR action spectrum of CHHP was recorded by scanning the OPO from 6990 to 7040 cm^{-1} at a scan speed of 0.1 cm^{-1} s^{-1} in the first overtone OH stretch ($2\nu_{OH}$) region under jet-cooled conditions, as shown in Fig. 2. The IR action spectrum is obtained with LIF detection of OH products on the A-X (1,0) $Q_1(3.5)$ transition at an IR-UV delay time of 700 ns (see Section S3 and Fig. S7 of the ESI†). This requires IR multiphoton excitation, which induces dissociation of CHHP and leads to formation of cyclohexoxy (RO) and OH products. The IR action spectrum exhibits a single prominent band at 7012.5 cm^{-1} with a full width at half maximum (FWHM) of *ca.* 7.5 cm^{-1}. The breadth of the observed feature is noticeably greater than the *ca.* 5 cm^{-1} FWHM band contour expected for an isolated vibrational overtone transition of CHHP under jet-cooled conditions. The

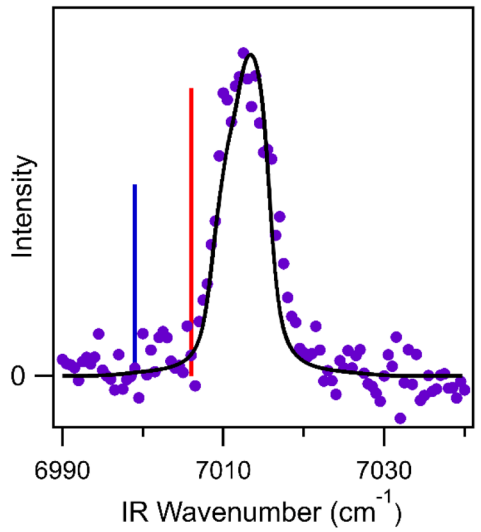

Fig. 2 Theoretically predicted $2\nu_{OH}$ transitions for the equatorial (red) and axial (blue) conformers of CHHP at 7006 and 6999 cm^{-1}, respectively, shown with relative intensities of 60 : 40 for a room temperature Boltzmann distribution. The experimental IR action spectrum (purple points) is overlaid with a simulated rotational band contour (black) for a scenario of closely spaced $2\nu_{OH}$ transitions (*ca.* 3 cm^{-1} apart) for equatorial and axial conformers. A nearly indistinguishable simulation results from an alternate limiting case with IR power broadening of the $2\nu_{OH}$ transition for the equatorial conformer that increases the homogeneous linewidth to 6.0 cm^{-1} (see Fig. S8†). The spectral shift of the observed feature (*ca.* 10 ± 2 cm^{-1}) is within the accuracy of the theoretical predictions (10–20 cm^{-1}).

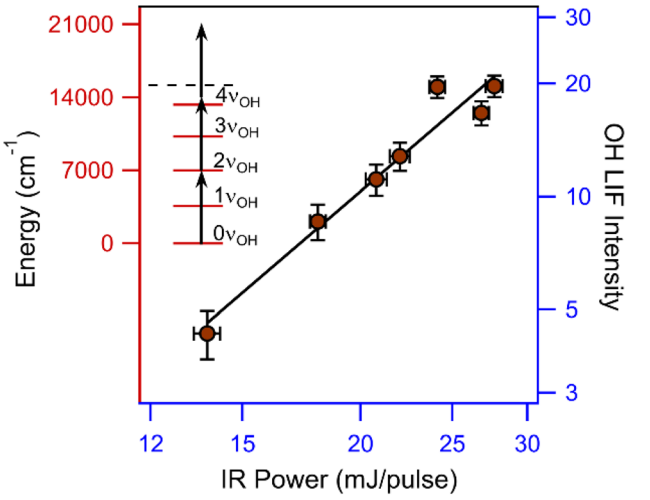

Fig. 3 (Left) Energy diagram showing the multiphoton dissociation of CHHP. IR excitation of the $2\nu_{OH}$ transition (black arrow) followed by absorption of additional photon(s) provides sufficient energy to exceed the O–O bond dissociation limit of CHHP (dashed line), resulting in cyclohexoxy and OH radicals. The OH radicals are detected using LIF on the $A^2\Sigma^+$–$X^2\Pi_{3/2}$ (1,0) $Q_1(3.5)$ transition at 282 nm. (Right) IR-induced OH LIF signal intensity at 7012.5 cm^{-1} as a function of IR power (mJ per pulse). Both axes are plotted on a $\log_{10}$ scale, yielding a slope of 2.3 ± 0.3. The nonlinear IR power dependence indicates multiphoton excitation of CHHP.

anticipated breadth is based on simulations using experimental rotational constants,[53] a rotational temperature of 10 K, the OPO bandwidth (0.9 cm^{-1}), and typical homogeneous broadening (1.7 cm^{-1}) associated with rapid (ps) intramolecular vibrational energy redistribution.[12,62]

The experimental observation of a single broadened feature at 7012.5 cm^{-1} can result from different population distributions for the equatorial and axial conformers of CHHP. One limiting case is a 60 : 40 population ratio of equatorial to axial conformers estimated for a Boltzmann distribution at 300 K and assumed to be unchanged upon supersonic expansion. In this case, the $2\nu_{OH}$ transitions for the equatorial and axial conformers would need to be more closely spaced, *e.g. ca.* 3 cm^{-1} apart, than predicted theoretically such that the two band contours merge into a single feature as shown in Fig. 2. An alternative limiting scenario is that the observed $2\nu_{OH}$ feature originates primarily from the lower energy equatorial conformer with IR power broadening increasing the homogeneous linewidth to 6.0 cm^{-1}. The two limiting cases yield nearly indistinguishable spectra as illustrated in Fig. S8.† The observed feature appears at higher energy (*ca.* 10 ± 2 cm^{-1}) than predicted for the equatorial and axial conformers (7006 and 6999 cm^{-1}, respectively), which is well within the accuracy of the theoretical predictions (10–20 cm^{-1}).

A previous study reported an extensively broadened $2\nu_{OH}$ feature (12.2 cm^{-1} FWHM) for TBHP under jet-cooled conditions, which was attributed to tunneling across the symmetric double-well potential along the OH torsion coordinate.[49,50] This resulted in multiple transitions and associated inhomogeneous broadening. Such broadening is not anticipated in CHHP since the double-well potential associated with OH torsion is asymmetric at the global minimum energy geometry of CHHP.

The IR power dependence of the $2\nu_{OH}$ transition of CHHP at 7012.5 cm^{-1} is obtained by varying the output power of the OPO from 13 to 28 mJ per pulse, as shown in Fig. 3 with both axes on a $\log_{10}$ scale. The variation of the OH LIF signal with IR laser power reveals a slope of 2.3 ± 0.3. The nonlinear dependence on IR power implies that the dissociation process requires multiphoton absorption of IR photons in the $2\nu_{OH}$ region. The slope indicates that more than two photons are required to promote CHHP above the dissociation limit, yielding the OH radicals that are detected. The energies of the OH fundamental and first overtone transitions are obtained from the VPT2 calculation, while the higher OH overtone levels ($3\nu_{OH}$ and $4\nu_{OH}$) illustrated in Fig. 3 are estimated from an anharmonic vibrational analysis.

Fig. 4 presents the CASPT2 relaxed potential energy (PE) profile along the O–O stretch coordinate (R_{OO}) for the equatorial conformer of CHHP. The PE profile shows a weak saddle point at R_{OO} = 2.78 Å followed by a shallow minimum at R_{OO} = 2.8 Å, the latter of which arises from a hydrogen bonding interaction between the O lone pair of the cyclohexoxy radical (RO) and the H-atom of the OH unit. The energy profile along the O–O coordinate beyond R_{OO} > 3.4 Å proceeds smoothly to the RO + OH asymptotic limit, which is consistent with earlier studies of other hydroperoxides.[63,64] The corresponding PE profile for the axial conformer of CHHP is shown in Fig. S9.† Using the asymptotic energies, bond dissociation energies (D_e) of *ca.*

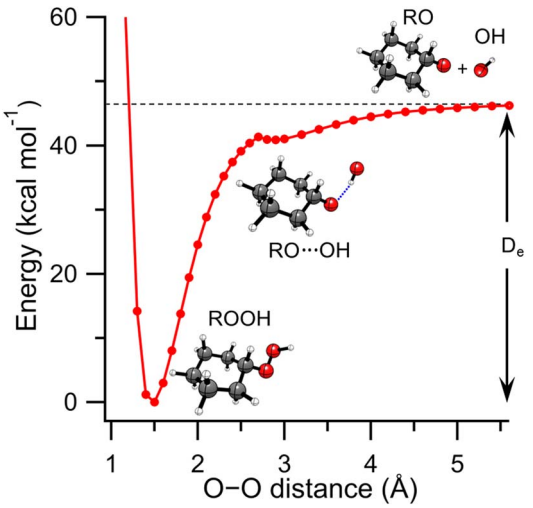

Fig. 4 Energy diagram for the equatorial conformer of CHHP (ROOH) along the O–O stretch coordinate (R_{OO}) to form cyclohexoxy (RO) + OH products. The potential is calculated at the CASPT2/aug-cc-pVTZ level of theory. A bond dissociation energy (D_e) of 46 kcal mol^{-1} is obtained for the equatorial conformer of CHHP.

46 kcal mol^{-1} are determined for both equatorial and axial conformers. Upon ZPE correction, the resulting D_0 values for both conformers are *ca.* 42 kcal mol^{-1}. The W1BD method predicts a D_0 value of 43 kcal mol^{-1} (Table 1), which agrees well with the ZPE-corrected CASPT2 energies. The W1BD method is known to give thermochemical quantities that are within chemical accuracy (1 kcal mol^{-1}).

Given that the IR excitation is tuned to 7012.5 cm^{-1} (*ca.* 20 kcal mol^{-1}), which corresponds to the $2\nu_{OH}$ transition of CHHP, multiphoton dissociation is required to initiate O–O bond fission. With a W1BD derived D_0 value of 43 kcal mol^{-1}, at least three photons of the OH first overtone transition would be required to promote O–O bond fission. The third photon would impart an excess energy of *ca.* 17 kcal mol^{-1} into CHHP, which upon intramolecular vibrational energy redistribution would provide sufficient energy in O–O stretch to promote O–O bond fission.

Table 1 Computed O–O dissociation energies (D_0, kcal mol^{-1}) for several hydroperoxides evaluated at various levels of theory and comparison with experiment

	This work		Bach *et al.*[a]		
	W1BD	CCSD(T)-F12/cc-pVTZ-F12[b]	CBS-APNO	G4	Expt.
HO–OH	48.4	48.1	50.2	49.0	50.30[c]
CH_3O–OH	41.9	42.4	44.6	43.2	44.67[c]
$(CH_3)_3CO$–OH	44.0	43.5	45.8	43.9	44.1[d]
$(CH_3)_2CHO$–OH	43.9	44.1	—	—	—
cyc–$C_6H_{11}O$–OH	43.4	—	—	—	—

[a] Ref. 52. [b] ZPE corrected with vibrational wavenumbers derived at the B2PLYP-D3/cc-pVTZ level. [c] Ref. 65. [d] Ref. 66.

The O–O bond dissociation energy (D_0) for CHHP (cyc–$C_6H_{11}O$–OH) is compared with those computed for four simpler hydroperoxides (ROOH) using the same W1BD method in Table 1. The D_0 values of the representative hydroperoxides are also evaluated with the CCSD(T)-F12/cc-pVTZ-F12 method (Table 1). The calculated dissociation energies using the W1BD and CCSD(T)-F12 methods compare favorably with those previously reported with the CBS-APNO and G4 methods.[52] Prior theoretical studies of O–O bond dissociation energies for ROOH with various substituents ranged from *ca.* 35 to 50 kcal mol^{-1} with a typical O–O bond dissociation energy of *ca.* 45 kcal mol^{-1}.[51,52]

The present calculations, along with those conducted previously,[51,52] show that the organic hydroperoxides have D_0(O–O) values that are *ca.* 4–7 kcal mol^{-1} lower than that of hydrogen peroxide. This can be qualitatively understood from the relative stabilities of the OH *vs.* RO radical products. Alkyl groups are well-known σ-electron donors and the H-atoms of the CH_3 moiety participate in hyperconjugation. Both effects are expected to stabilize the oxygen-centered odd-electron (the electron deficient p-orbital) of the RO radical. Equivalent stabilizations are not available for OH, resulting in more stable OR radicals. Interestingly, the organic hydroperoxide with a primary carbon-center (CH_3O–OH) has a D_0 value that is *ca.* 1–2 kcal mol^{-1} lower than that of secondary [$(CH_3)_2CHO$–OH and cyc–$C_6H_{11}O$–OH] and tertiary ($(CH_3)_3CO$–OH) carbon-centered hydroperoxides. The secondary and tertiary carbon-centers are more electron-rich than primary carbon-centers due to the +I inductive effects imparted by the alkyl-substituents; this is expected to increase the nucleophilicity of the carbon-center. Additionally, hyperconjugation is not available in the secondary and tertiary carbon centers. Both effects are expected to destabilize secondary and tertiary carbon-centered organic hydroperoxides, consistent with their higher bond dissociation energies.

4 Conclusions

A new synthetic approach for generating CHHP is utilized in the present study of its IR spectroscopy and multiphoton dissociation dynamics. The IR spectrum of jet-cooled CHHP has been recorded in the first overtone OH stretch ($2\nu_{OH}$) region. Quantum chemical studies reveal that the equatorial conformer of CHHP is slightly more stable than the axial conformer (*ca.* 0.2 kcal mol^{-1}) and separated by a substantial TS barrier for isomerization (*ca.* 11.5 kcal mol^{-1}). As a result, both conformers may be populated under jet-cooled conditions, in accord with a recent rotational spectroscopy investigation.[53] IR multiphoton excitation promotes CHHP above the O–O dissociation limit, resulting in OH $X^2\Pi$ ($v = 0$) radical products that are detected *via* UV-LIF. IR action spectroscopy yields a distinctive, yet broadened, vibrational overtone feature for CHHP at 7012.5 cm^{-1}. This can be ascribed to various scenarios ranging from a single homogeneously broadened feature dominated by the equatorial conformer to overlapping band contours for the equatorial and axial conformers that merge into a single feature. The nonlinear IR power dependence of this spectral

feature confirms that a minimum of three photons with energies corresponding to $2\nu_{OH}$ are required to promote O–O bond fission. This observation is confirmed by computation of relaxed CASPT2 potential energy profiles along the O–O bond stretch coordinate for the equatorial and axial conformers, and determination of the O–O bond dissociation energy using the W1BD method.

The present study adds to the small but growing body of work on larger organic hydroperoxides. In the future, we anticipate the emergence of synthetic procedures for laboratory investigation of the spectroscopy and dissociation dynamics of more complex and atmospherically relevant organic hydroperoxides.

Data availability

All supporting data and methods are available in the ESI.†

Author contributions

M. I. L. and T. N. V. K. designed the experimental and theoretical aspects of the research project, respectively. C. S. and M. C. K. synthesized cyclohexyl hydroperoxide (CHHP). T. K. R and Y. Q. conducted the experiments and analyzed the experimental data. L. K., R. R., and T. N. V. K. carried out the theoretical calculations. All authors discussed the results and contributed to writing the manuscript.

Conflicts of interest

There are no conflicts to declare.

Acknowledgements

Research in the Lester laboratory was supported by the National Science Foundation under grants CHE-1955068 and CHE-2301298. M. C. K. is grateful to the NSF (CHE-2102626) for financial support of this research. Partial instrumentation support (NMR spectrometer) was provided by NSF CHE-1827457 and the Vagelos Institute for Energy Science and Technology. T. K. R. was primarily supported by a Walter-Benjamin Scholarship funded by the Deutsche Forschungsgemeinschaft (DFG, German Research Foundation) – Project number 508074809. T. N. V. K. is grateful to the NSF (OIA-2229695) for financial support. This work used the Advanced Cyberinfrastructure Coordination Ecosystem: Service & Support (ACCESS) program, which is supported by National Science Foundation grants #2138259, #2138286, #2138307, #2137603, and #2138296, through the allocation TG-CHE190088.

References

1 S. Enami, Fates of Organic Hydroperoxides in Atmospheric Condensed Phases, *J. Phys. Chem. A*, 2021, **125**, 4513–4523.
2 F. Bianchi, O. Garmash, X. He, C. Yan, S. Iyer, I. Rosendahl, Z. Xu, M. P. Rissanen, M. Riva, R. Taipale, N. Sarnela, T. Petäjä, D. R. Worsnop, M. Kulmala, M. Ehn and H. Junninen, The role of highly oxygenated molecules (HOMs) in determining the composition of ambient ions in the boreal forest, *Atmos. Chem. Phys.*, 2017, **17**, 13819–13831.
3 L. Vereecken and B. Nozière, H-migration in peroxy radicals under atmospheric conditions, *Atmos. Chem. Phys.*, 2020, **20**, 7429–7458.
4 J. Lelieveld, T. M. Butler, J. N. Crowley, T. J. Dillon, H. Fischer, L. Ganzeveld, H. Harder, M. G. Lawrence, M. Martinez, D. Taraborrelli and J. Williams, Atmospheric oxidation capacity sustained by a tropical forest, *Nature*, 2008, **452**, 737–740.
5 D. L. Osborn, Reaction mechanisms on multiwell potential energy surfaces in combustion (and atmospheric) chemistry, *Annu. Rev. Phys. Chem.*, 2017, **68**, 233–260.
6 J. D. Savee, E. Papajak, B. Rotavera, H. Huang, A. J. Eskola, O. Welz, L. Sheps, C. A. Taatjes, J. Zádor and D. L. Osborn, Direct observation and kinetics of a hydroperoxyalkyl radical (QOOH), *Science*, 2015, **347**, 643–646.
7 L. Vereecken and J. S. Francisco, Theoretical studies of atmospheric reaction mechanisms in the troposphere, *Chem. Soc. Rev.*, 2012, **41**, 6259–6293.
8 G. Meloni, P. Zou, S. J. Klippenstein, M. Ahmed, S. R. Leone, C. A. Taatjes and D. L. Osborn, Energy-Resolved Photoionization of Alkylperoxy Radicals and the Stability of Their Cations, *J. Am. Chem. Soc.*, 2006, **128**, 13559–13567.
9 W. P. L. Carter, A detailed mechanism for the gas-phase atmospheric reactions of organic compounds, *Atmos. Environ. Part A. General Topics*, 1990, **24**, 481–518.
10 R. Atkinson, D. L. Baulch, R. A. Cox, R. F. Hampson Jr, J. A. Kerr, M. J. Rossi and J. Troe, Evaluated Kinetic, Photochemical and Heterogeneous Data for Atmospheric Chemistry: Supplement V. IUPAC Subcommittee on Gas Kinetic Data Evaluation for Atmospheric Chemistry, *J. Phys. Chem. Ref. Data*, 1997, **26**, 521–1011.
11 A. S. Hansen, T. Bhagde, K. B. Moore, D. R. Moberg, A. W. Jasper, Y. Georgievskii, M. F. Vansco, S. J. Klippenstein and M. I. Lester, Watching a hydroperoxyalkyl radical (•QOOH) dissociate, *Science*, 2021, **373**, 679–682.
12 A. S. Hansen, T. Bhagde, Y. Qian, A. Cavazos, R. M. Huchmala, M. A. Boyer, C. F. Gavin-Hanner, S. J. Klippenstein, A. B. McCoy and M. I. Lester, Infrared spectroscopic signature of a hydroperoxyalkyl radical (•QOOH), *J. Chem. Phys.*, 2022, **156**, 014301.
13 T. Bhagde, A. S. Hansen, S. Chen, P. J. Walsh, S. J. Klippenstein and M. I. Lester, Energy-resolved and time-dependent unimolecular dissociation of hydroperoxyalkyl radicals (•QOOH), *Faraday Discuss.*, 2022, **238**, 575–588.
14 J. D. Crounse, L. B. Nielsen, S. Jørgensen, H. G. Kjaergaard and P. O. Wennberg, Autoxidation of Organic Compounds in the Atmosphere, *J. Phys. Chem. Lett.*, 2013, **4**, 3513–3520.
15 M. Ehn, J. A. Thornton, E. Kleist, M. Sipilä, H. Junninen, I. Pullinen, M. Springer, F. Rubach, R. Tillmann, B. Lee, F. Lopez-Hilfiker, S. Andres, I.-H. Acir, M. Rissanen, T. Jokinen, S. Schobesberger, J. Kangasluoma,

J. Kontkanen, T. Nieminen, T. Kurtén, L. B. Nielsen, S. Jørgensen, H. G. Kjaergaard, M. Canagaratna, M. D. Maso, T. Berndt, T. Petäjä, A. Wahner, V.-M. Kerminen, M. Kulmala, D. R. Worsnop, J. Wildt and T. F. Mentel, A large source of low-volatility secondary organic aerosol, *Nature*, 2014, **506**, 476–479.

16 T. Jokinen, M. Sipilä, S. Richters, V.-M. Kerminen, P. Paasonen, F. Stratmann, D. Worsnop, M. Kulmala, M. Ehn, H. Herrmann and T. Berndt, Rapid Autoxidation Forms Highly Oxidized RO_2 Radicals in the Atmosphere, *Angew. Chem., Int. Ed.*, 2014, **53**, 14596–14600.

17 T. Berndt, S. Richters, T. Jokinen, N. Hyttinen, T. Kurtén, R. V. Otkjær, H. G. Kjaergaard, F. Stratmann, H. Herrmann, M. Sipilä, M. Kulmala and M. Ehn, Hydroxyl radical-induced formation of highly oxidized organic compounds, *Nat. Commun.*, 2016, **7**, 13677.

18 E. Praske, R. V. Otkjær, J. D. Crounse, J. C. Hethcox, B. M. Stoltz, H. G. Kjaergaard and P. O. Wennberg, Atmospheric autoxidation is increasingly important in urban and suburban North America, *Proc. Natl. Acad. Sci. U.S.A.*, 2018, **115**, 64–69.

19 D. J. Medeiros, M. A. Blitz, P. W. Seakins and L. K. Whalley, Direct Measurements of Isoprene Autoxidation: Pinpointing Atmospheric Oxidation in Tropical Forests, *J. Am. Chem. Soc.*, 2022, **2**, 809–818.

20 M. Ge, S. Tong, W. Wang, W. Zhang, M. Chen, C. Peng, J. Li, L. Zhou, Y. Chen and M. Liu, Important Oxidants and Their Impact on the Environmental Effects of Aerosols, *J. Phys. Chem. A*, 2021, **125**, 3813–3825.

21 C. Li and R. Signorell, Understanding vapor nucleation on the molecular level: A review, *J. Aerosol Sci.*, 2021, **153**, 105676.

22 V. F. McNeill, Virtual Special Issue: New Advances in Organic Aerosol Chemistry, *ACS Earth Space Chem.*, 2020, **4**, 491–494.

23 E. W. Kaiser, Temperature and Pressure Dependence of the C_2H_4 Yield from the Reaction $C_2H_5 + O_2$, *J. Phys. Chem.*, 1995, **99**, 707–711.

24 E. W. Kaiser, Formation of C_3H_6 from the Reaction $C_3H_7 + O_2$ between 450 and 550 K, *J. Phys. Chem. A*, 1998, **102**, 5903–5906.

25 E. W. Kaiser and T. J. Wallington, Formation of C3H6 from the Reaction $C_3H_7 + O_2$ and C_2H_3Cl from $C_2H_4Cl + O_2$ at 297 K, *J. Phys. Chem.*, 1996, **100**, 18770–18774.

26 I. C. Plumb and K. R. Ryan, Kinetic studies of the reaction of C_2H_5 with O_2 at 295 K, *Int. J. Chem. Kinet.*, 1981, **13**, 1011–1028.

27 E. P. Clifford, J. T. Farrell, J. D. DeSain and C. A. Taatjes, Infrared Frequency-Modulation Probing of Product Formation in Alkyl + O_2 Reactions: I. The Reaction of C_2H_5 with O_2 between 295 and 698 K, *J. Phys. Chem. A*, 2000, **104**, 11549–11560.

28 J. D. DeSain, E. P. Clifford and C. A. Taatjes, Infrared Frequency-Modulation Probing of Product Formation in Alkyl + O_2 Reactions: II. The Reaction of C_3H_7 with O_2 between 296 and 683 K, *J. Phys. Chem. A*, 2001, **105**, 3205–3213.

29 J. D. DeSain, C. A. Taatjes, J. A. Miller, S. J. Klippenstein and D. K. Hahn, Infrared frequency-modulation probing of product formation in alkyl + O_2 reactions. Part IV. Reactions of propyl and butyl radicals with O_2, *Faraday Discuss.*, 2002, **119**, 101–120.

30 E. W. Kaiser, I. M. Lorkovic and T. J. Wallington, Pressure dependence of the ethene yield from the reaction ethyl radical + oxygen, *J. Phys. Chem.*, 1990, **94**, 3352–3354.

31 E. G. Estupiñán, J. D. Smith, A. Tezaki, S. J. Klippenstein and C. A. Taatjes, Measurements and Modeling of DO_2 Formation in the Reactions of C_2D_5 and C_3D_7 Radicals with O_2, *J. Phys. Chem. A*, 2007, **111**, 4015–4030.

32 J. Zádor, C. A. Taatjes and R. X. Fernandes, Kinetics of elementary reactions in low-temperature autoignition chemistry, *Prog. Energy Combust. Sci.*, 2011, **37**, 371–421.

33 J. J. Orlando and G. S. Tyndall, Laboratory studies of organic peroxy radical chemistry: an overview with emphasis on recent issues of atmospheric significance, *Chem. Soc. Rev.*, 2012, **41**, 6294–6317.

34 R. W. Walker and C. Morley, Chapter 1 Basic chemistry of combustion, In *Comprehensive Chemical Kinetics*, ed. M. J. Pilling, Elsevier, 1997, vol. 35, pp. 1–124.

35 S. Sharma, S. Raman and W. H. Green, Intramolecular Hydrogen Migration in Alkylperoxy and Hydroperoxyalkylperoxy Radicals: Accurate Treatment of Hindered Rotors, *J. Phys. Chem. A*, 2010, **114**, 5689–5701.

36 J. D. DeSain and C. A. Taatjes, Infrared Frequency-Modulation Probing of Product Formation in Alkyl + O_2 Reactions: III. The Reaction of Cyclopentyl Radical (c-C_5H_9) with O_2 between 296 and 723 K, *J. Phys. Chem. A*, 2001, **105**, 6646–6654.

37 H. R. Dübal and F. F. Crim, Vibrational overtone predissociation spectroscopy of hydrogen peroxide, *J. Chem. Phys.*, 1985, **83**, 3863–3872.

38 T. M. Ticich, M. D. Likar, H. R. Dübal, L. J. Butler and F. F. Crim, Vibrationally mediated photodissociation of hydrogen peroxide, *J. Chem. Phys.*, 1987, **87**, 5820–5829.

39 D. T. Colbert and E. L. Sibert III, Theory of vibrationally mediated photodissociation of HOOH: Delocalized tails in a localized wave function, *J. Chem. Phys.*, 1991, **94**, 6519–6545.

40 M. D. Likar, J. E. Baggott and F. F. Crim, Vibrationally mediated photodissociation of t-butyl hydroperoxide: Vibrational overtone spectroscopy and photodissociation dynamics, *J. Chem. Phys.*, 1989, **90**, 6266–6274.

41 M. D. Likar, J. E. Baggott, A. Sinha, T. M. Ticich, R. L. V. Wal and F. F. Crim, Vibrationally mediated photodissociation, *J. Chem. Soc., Faraday Trans. 2*, 1988, **84**, 1483–1497.

42 M. Brouard, M. T. Martinez, J. O'Mahony and J. P. Simons, Energy and angular momentum disposals in the vibrationally mediated photodissociation of HOOH and HOOD, *Mol. Phys.*, 1990, **69**, 65–84.

43 J. August, M. Brouard, M. P. Docker, C. J. Milne, J. P. Simons, R. Lavi, S. Rosenwaks and D. Schwartz-Lavi, Photodissociation dynamics of tert-butyl nitrite (S2) and tert-butyl hydroperoxide at 248-250 nm, *J. Phys. Chem.*, 1988, **92**, 5485–5491.

44 Y. Inagaki, Y. Matsumi and M. Kawasaki, Formation of a Hydrogen Atom from the Photodissociation of Hydrogen Peroxide at 193 nm, *Bull. Chem. Soc. Jpn.*, 1993, **66**, 3166–3170.

45 S. K. Shin, S. O. Park, Y. S. Choi, H. L. Kim and C. R. Park, Photodissociation Dynamics of Cumene Hydroperoxide at 248 and 193 nm, *J. Phys. Chem. A*, 2001, **105**, 10018–10024.

46 B.-G. Ryu, C. R. Park, Y. Lee, S. K. Shin and H. L. Kim, Photodissociation dynamics of tert-butyl hydroperoxide at 266 nm, *J. Photochem. Photobiol.*, 2002, **149**, 15–21.

47 S. Hsieh, R. Vushe, Y. T. Tun and J. L. Vallejo, Trends in organic hydroperoxide photodissociation and absorption cross sections between 266 and 377nm, *Chem. Phys. Lett.*, 2014, **591**, 99–102.

48 M. D. Likar, J. E. Baggott and F. F. Crim, Vibrationally mediated photodissociation of t-butyl hydroperoxide: Vibrational overtone spectroscopy and photodissociation dynamics, *J. Chem. Phys.*, 1989, **90**, 6266–6274.

49 A. S. Hansen, R. M. Huchmala, E. Vogt, M. A. Boyer, T. Bhagde, M. F. Vansco, C. V. Jensen, A. Kjærsgaard, H. G. Kjaergaard, A. B. McCoy and M. I. Lester, Coupling of torsion and OH-stretching in tert-butyl hydroperoxide. I. The cold and warm first OH-stretching overtone spectrum, *J. Chem. Phys.*, 2021, **154**, 164306.

50 E. Vogt, R. M. Huchmala, C. V. Jensen, M. A. Boyer, J. Wallberg, A. S. Hansen, A. Kjærsgaard, M. I. Lester, A. B. McCoy and H. G. Kjaergaard, Coupling of torsion and OH-stretching in tert-butyl hydroperoxide. II. The OH-stretching fundamental and overtone spectra, *J. Chem. Phys.*, 2021, **154**, 164307.

51 R. D. Bach, P. Y. Ayala and H. B. Schlegel, A Reassessment of the Bond Dissociation Energies of Peroxides. An ab Initio Study, *J. Am. Chem. Soc.*, 1996, **118**, 12758–12765.

52 R. D. Bach and H. B. Schlegel, Bond Dissociation Energy of Peroxides Revisited, *J. Phys. Chem. A*, 2020, **124**, 4742–4751.

53 P. Pinacho, W. Sun, D. A. Obenchain and M. Schnell, Conformational analysis of cyclohexyl hydroperoxide by rotational spectroscopy, *J. Mol. Spectrosc.*, 2023, **392**, 111758.

54 Z. Hu, Q. Di, B. Liu, Y. Li, Y. He, Q. Zhu, Q. Xu, P. Dagaut, N. Hansen, S. M. Sarathy, L. Xing, D. G. Truhlar and Z. Wang, Elucidating the photodissociation fingerprint and quantifying the determination of organic hydroperoxides in gas-phase autoxidation, *Proc. Natl. Acad. Sci. U.S.A.*, 2023, **120**, e2220131120.

55 J. B. Sperry, M. Azuma and S. Stone, Explosive Hazard Identification in Pharmaceutical Process Development: A Novel Screening Method and Workflow for Shipping Potentially Explosive Materials, *Org. Process Res. Dev.*, 2021, **25**, 212–224.

56 T. Tokuyasu, S. Kunikawa, A. Masuyama and M. Nojima, Co(III)−Alkyl Complex- and Co(III)−Alkylperoxo Complex-Catalyzed Triethylsilylperoxidation of Alkenes with Molecular Oxygen and Triethylsilane, *Org. Lett.*, 2002, **4**, 3595–3598.

57 E. C. Barnes, G. A. Petersson, J. A. Montgomery Jr, M. J. Frisch and J. M. L. Martin, Unrestricted Coupled Cluster and Brueckner Doubles Variations of W1 Theory, *J. Chem. Theory Comput.*, 2009, **5**, 2687–2693.

58 M. J. Frisch, G. W. Trucks, H. B. Schlegel, G. E. Scuseria, M. A. Robb, J. R. Cheeseman, G. Scalmani, V. Barone, G. A. Petersson, H. Nakatsuji and *et al.*, *Gaussian 16, Rev. C.01*, Gaussian, Inc., Wallingford, CT, 2016.

59 H.-J. Werner, P. J. Knowles, G. Knizia, F. R. Manby, M. Schütz, P. Celani, W. Györffy, D. Kats, T. Korona, R. Lindh, *et.al.*, *MOLPRO 2020.1, a package of ab initio programs*, 2020, see **https://www.molpro.net**.

60 H.-J. Werner, P. J. Knowles, G. Knizia, F. R. Manby and M. Schütz, Molpro: a general-purpose quantum chemistry program package, *Wiley Interdiscip. Rev.: Comput. Mol. Sci.*, 2012, **2**, 242–253.

61 H.-J. Werner, P. J. Knowles, F. R. Manby, J. A. Black, K. Doll, A. Heßelmann, D. Kats, A. Köhn, T. Korona, D. A. Kreplin, Q. Ma, T. F. Miller, A. Mitrushchenkov, K. A. Peterson, I. Polyak, G. Rauhut and M. Sibaev, The Molpro quantum chemistry package, *J. Chem. Phys.*, 2020, **152**, 144107.

62 A. S. Hansen, Y. Qian, C. A. Sojdak, M. C. Kozlowski, V. J. Esposito, J. S. Francisco, S. J. Klippenstein and M. I. Lester, Rapid Allylic 1,6 H-Atom Transfer in an Unsaturated Criegee Intermediate, *J. Am. Chem. Soc.*, 2022, **144**, 5945–5955.

63 N. M. Kidwell, H. Li, X. Wang, J. M. Bowman and M. I. Lester, Unimolecular dissociation dynamics of vibrationally activated CH_3CHOO Criegee intermediates to OH radical products, *Nat. Chem.*, 2016, **8**, 509–514.

64 B. Marchetti, V. J. Esposito, R. E. Bush and T. N. V. Karsili, The states that hide in the shadows: the potential role of conical intersections in the ground state unimolecular decay of a Criegee intermediate, *Phys. Chem. Chem. Phys.*, 2022, **24**, 532–540.

65 *Active Thermochemical Tables*, **https://atct.anl.gov/Thermochemical/Data/version-1.130/index.php**, (accessed February 2024).

66 W. Reints, D. A. Pratt, H.-G. Korth and P. Mulder, O−O Bond Dissociation Enthalpy in Di(trifluoromethyl) Peroxide (CF_3OOCF_3) as Determined by Very Low Pressure Pyrolysis. Density Functional Theory Computations on O−O and O−H Bonds in (Fluorinated) Derivatives, *J. Phys. Chem. A*, 2000, **104**, 10713–10720.